RSC Advances

PAPER

View Article Online
View Journal | View Issue

Cite this: *RSC Adv.*, 2016, **6**, 2800

Implications for blood-brain-barrier permeability, *in vitro* oxidative stress and neurotoxicity potential induced by mesoporous silica nanoparticles: effects of surface modification†

Ming Zhou,‡[a] Linlin Xie,‡[a] Chen-Jie Fang,*[a] Hua Yang,[b] Yan-Jie Wang,[c] Xiao-Yu Zhen,[c] Chun-Hua Yan,*[c] Yuji Wang,[a] Ming Zhao*[ad] and Shiqi Peng*[a]

The increase in the abundance and practical applications of nanomaterials has led to growing concern over the potential adverse effects of nanoparticles on human health. Their unique structure makes mesoporous silica nanoparticles (MSNs) an ideal platform for developing multifunctional nanocarriers, including non-viral gene delivery in the central nervous system (CNS). However, the potential neurotoxicity of the MSNs remains largely unclear. In this study, we explored the biological effect of MCM-41 type MSNs on blood-brain-barrier (BBB) permeability, neuronal damage, and the mediation of neurotoxicity with surface chemistry. With or without the ligand transferrin (Tf), which could interact with the transferrin receptor expressed at the BBB, *in vivo* imaging indicated that both MSN–Cy–Tf and MSN–Cy may enter into the brain, suggesting their potential to deliver therapeutic agents across the BBB. However, a risk arises that is associated with this permeability. A histological observation of the hippocampus confirms the CNS delivery of MSNs and indicates neuronal damage, characterized by neuronal cell loss, nuclei shrinkage, and the disintegration of neurons, suggestive of *in vivo* neurotoxicity. With the PC12 cell, a model for the dopaminergic neuron, an *in vitro* examination suggests that various surface modified MSNs decrease the cell viability and cause oxidative stress with an elevation of reactive oxygen species (ROS), a depletion of glutathione (GSH), leakage of lactate dehydrogenase (LDH), and the generation of malondialdehyde (MDA) in a concentration-dependent manner. Compared with the pristine MSNs which induce the severest injury impact on the cells, thiol modified MSN–SH nanoparticles show significantly lower injury effects among the test MSNs, suggesting the possibility to mediate the neurotoxicity by modifying the surface chemistry of this kind of the nanomaterial for biomedical applications.

Received 29th August 2015
Accepted 8th December 2015

DOI: 10.1039/c5ra17517h

www.rsc.org/advances

1. Introduction

The blood-brain-barrier (BBB) is the strongest biological barrier and protects the brain. For more than 98% of drugs treating central nervous system (CNS) disorders, however, this barrier is also a formidable obstacle for the effective delivery of the therapeutic agents to the brain. Therefore, there is a clear need for various strategies to deliver non-permeating CNS therapeutic agents to the brain.[1,2] Within the advancing nanomaterials, nanoparticles would be an efficient alternative for drug delivery to the brain. However the interactions of nanomaterials with various biological systems and barriers, especially the BBB, as well as the toxicological/biological effect of nanomaterials, are still largely unknown.[3] Up to date, only limited works show that the deposition of nanomaterials in the brain can cause oxidative stress, tissue damage, and neurotoxicity,[4,5] whereas the precise pathway and mechanism of neuronal damage remains principally unclear.

Brain tissue is mainly composed of neurons and glial cells. As core cells, neurons are critical for brain function. Neuronal damage, including defects of the structure and/or the loss of function, plays a crucial role in aging and some neurodegenerative diseases, such as Parkinson's disease and Alzheimer's

[a]*Beijing Area Major Laboratory of Peptide and Small Molecular Drugs, Engineering Research Center of Endogenous Prophylactic of Ministry of Education of China, Beijing Laboratory of Biomedical Materials, College of Pharmaceutical Sciences, Capital Medical University, Beijing 100069, P. R. China. E-mail: sqpeng@ccmu.edu.cn*

[b]*Medical Experimental & Test Centre, Capital Medical University, Beijing 100069, China*

[c]*Beijing National Laboratory for Molecular Sciences, State Key Laboratory of Rare Earth Materials Chemistry and Applications, PKU-HKU Joint Laboratory on Rare Earth Materials and Bioinorganic Chemistry, Peking University, Beijing 100871, China*

[d]*Faculty of Biomedical Science and Environmental Biology, Kaohsiung Medical University, Kaohsiung, Taiwan*

† Electronic supplementary information (ESI) available: Additional materials characterization technique (Fig. S1). Images of the deep brain slices (Fig. S2). Correlation plot of the levels of ROS, GSH, and MDA *versus* the level of LDH for various MSNs. See DOI: 10.1039/c5ra17517h

‡ These authors contributed equally to this work.

disease. Due to the large amount of oxygen consumed and oxidant production along with antioxidant deficiency, the brain and CNS are particularly susceptible to oxidative stress induced by reactive oxygen species (ROS).[6,7] The oxidants derived from ROS, such as H_2O_2 and $OH^{\bullet -}$, are highly reactive toward DNA, proteins, and lipids, causing significant destruction to cells.[8,9] As essential physiological regulators, ROS normally exists in cells in balance with antioxidants.[10] Excessive oxidants will induce lipid peroxidation, DNA damage, and tissue toxicity.[11]

Since Mobil researchers reported the synthesis of mesoporous silica,[12] a burgeoning area of porous silica research, especially for mesoporous silica nanoparticles (MSNs), has been their use as nanocarriers in the applications of therapy and diagnosis.[13,14] MSNs possess unique structural characteristics such as a large surface area, tunable pore size and channel, and well-defined surface properties, which make MSNs an ideal platform for drug delivery[15–19] and further leads to substantial research regarding their chemical stability, biodistribution and excretion, biocompatibility and biosafety.[16,20–22] While the beneficial aspects are widely publicized, some new concerns including the negative impact of the MSNs on living cells and tissues have arisen. It is still unknown whether the MSNs could enter the brain and exert adverse effects, and how the MSNs interact with the brain tissues and neurons.

Although the toxicity of silicon and silica has been continually studied for more than a century,[23–30] little is known about the possible adverse effects on the brain once silica enters the CNS. As silica nanoparticles (SiNPs) are generally deemed nontoxic, SiNPs have been formulated for non-viral gene delivery in the CNS.[31,32] However, when Guilarte *et al.* first examined the effects of SiNP (150 to 200 nm) exposure on the brain using primary rat microglia the results suggested that very low levels of SiNPs increase ROS production and are capable of altering the microglial function.[33] Wu *et al.* demonstrated that SiNPs (15 nm) possibly have a negative impact on the striatum and dopaminergic neurons as well being a potential risk for neurodegenerative diseases.[34] To the best of our knowledge, so far no study has been carried out to define the effects of MSNs on BBB permeability, neuronal damage and oxidative stress. Because a high surface-to-volume ratio of nanomaterials could create more potential for enhanced cellular interactions and different pathways of toxicity compared with coarse grained silica,[26,35–37] it is urgent to explore the (neuro)toxicity of ordered MSNs and the relationship with the nanoparticles' physicochemical properties.[26,38–40] In this context, we explored the *in vivo* BBB permeability, neuronal damage, and *in vitro* oxidative stress induced by MSNs with different surface groups (Chart 1).

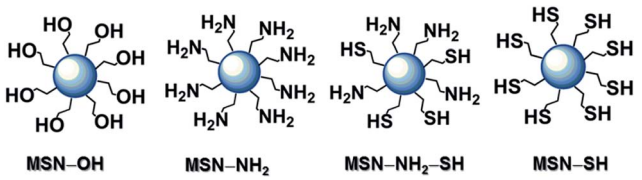

Chart 1 MSNs with only silanol residues (MSN–OH) and surface modified MSN–NH_2, MSN–NH_2–SH, and MSN–SH.

2. Experimental section

2.1 Synthesis and characterization of the MSNs

MSN–NH_2, MSN–NH_2–SH, and MSN–SH were synthesized by a co-condensation method according to our previous work.[41,42] For MSN–Cy, the fluorescent dye Cy5.5 was attached covalently to MSN–NH_2 *via* amide bonds. Then transferrin (Tf) was attached covalently to MSN–Cy at room temperature in the dark overnight to fabricate MSN–Cy–Tf. The nanoparticles were collected by centrifugation, and the supernatant was collected for analysis. The particles were then washed and sonicated several times in order to remove any adsorbed protein and then dried under vacuum.

Powder X-ray diffraction (XRD) patterns of the nanoparticles were recorded on a Rigaku D/Max-2000 X-ray powder diffractometer (Japan) using Cu K_α (λ = 1.5405 Å) radiation. TEM images were taken on a JEM-2100 transmission electron microscope under a working voltage of 200 kV. The nitrogen adsorption and desorption isotherms were measured on an ASAP 2010 analyser (Micromeritics Co. Ltd.) at 78 K. The surface charge of the nanoparticles was measured with a zetasizer (NanoZS Malvern Inst., Malvern, UK). The size distribution was also measured using dynamic light scattering (DLS) with the zetasizer.

2.2 *In vivo* animal studies

The animal studies were approved by the Animal Ethical Committee of Capital Medical University (China). Six-week-old male nude mice were purchased from the Weitonglihua Laboratory Animal Co., Ltd. (Beijing, China). Six mice per cage were housed under standard laboratory conditions (12 h light: 12 h dark and 24 ± 3 °C); rodent food and water were provided ad libitum. The experiments were initiated one week after the arrival of the animals.

2.2.1 *In vivo* imaging. Fluorescence from Cy5.5 attached to MSN–Cy and MSN–Cy–Tf in mice was obtained using a NightOWL LB983 *in vivo* imaging system (Berthold Technologies, Germany; excitation: 635–675 nm, emission: 695–740 nm), which was equipped with a cooled backside illuminated NightOWL II CCD camera, along with image acquisition and analysis software (IndiGO software). The fluorescence intensity of MSN–Cy and MSN–Cy–Tf was height-corrected.

2.2.2 Hematoxylin and eosin (H & E) staining. After exposure to MSN–Cy and MSN–Cy–Tf for 0.5 h, the mice were sacrificed by decapitation and their brains were dissected and immersed in 4% paraformaldehyde, fixed at 4 °C for at least 24 h, and then processed by routine histological methods. The coronary slices (5 μm) were obtained and used for hematoxylin and eosin (H & E) staining in accordance with the standard procedure. The eosin imparts a pink to red color to cytoplasm, and the hematoxylin stains the nucleus blue. The slices were observed on an Olympus SZX-MDHSW microscope (Japan) and photographed.

2.3 *In vitro* studies

2.3.1 Cell culture and differentiation. A PC12 cell line was obtained from the Beijing Xiehe Cell Bank of Type Culture

Collection. The cells were grown in a RPMI 1640 medium (Hyclone, USA) containing 5% fetal bovine serum (FBS), 100 U mL^{-1} penicillin, 100 μg mL^{-1} streptomycin, 10% horse serum, and 50 ng mL^{-1} nerve growth factor at 37 °C in an atmosphere of 5% CO_2.

The stock solution of the MSNs was prepared serially from 1 to 200 μg mL^{-1} of the samples. These samples were sonicated before exposure to the mice and cells to produce a less aggregated, uniform suspension. For the *in vitro* experiments, the freshly dispersed MSN suspensions were immediately applied to the cells. Cells free of the MSNs were used as the control.

2.3.2 MTT assay. The cytotoxicity of the MSNs was evaluated with a standard MTT (3-(4,5-dimethylthiazol-2-yl)-2,5-diphenyl-2*H*-tetrazolium bromide) assay. Briefly, PC12 cells were planted in 96-well plates (Corning, Inc., New York, USA) at a density of 2×10^4 cells per well in growth medium RPMI 1640. After 24 h incubation, the MSNs of various concentrations were loaded into the 96-well plates, and the viability of the PC12 cells was determined. 100 μL of MTT was added into each well and incubated for 4 h until purple crystals were visible. After removal of the MTT solution, the purple formazan crystals were dissolved in 100 μL of DMSO and the absorbance was measured at 490 nm on a microplate reader (BIO-RAD Model1680, USA). The cytotoxicity was expressed as the % of inhibition rate.

2.3.3 Intracellular ROS determination. DCFH-DA is a membrane-permeant compound and, once inside the cells, it is deacetylated by endogenous esterases to form the non-fluorescent 2′,7′-dichlorofluorescein (DCFH). DCFH is converted to fluorescent dichlorofluorescein (DCF) by cellular oxidation. As a result, green fluorescence is emitted in response to ROS production and can be analyzed by flow cytometry. Briefly, DCFH-DA (Sigma) was re-suspended in DMSO. The cells were incubated with DCFH-DA solution at a final concentration of 10 μM in RPMI 1640 without serum for 30 min at 37 °C in a 5% CO_2 atmosphere. Afterward, the cells were rinsed twice with PBS and centrifuged, and then the supernatant was discarded to collect the pellets. The pellets were re-suspended in PBS, and the data were collected using the Becton-Dickinson FACS Aria flow cytometer ($\lambda_{Ex}/\lambda_{Em}$ = 488/525 nm) and analyzed with BD-FACS Diva 4.1 software. The ROS level was expressed as the ratio of the mean intensity of the treated group *versus* the mean intensity of the control group.

2.3.4 Intracellular glutathione (GSH) measurement. The intracellular GSH content was measured with a glutathione assay kit (Sigma-Aldrich, USA). Briefly, PC12 cells were plated in six-well plates at a density of 5.0×10^5 cells per well and treated with various suspensions of the MSNs. After 24 h treatment, the cells were first deproteinized with 5% 5-sulfosalicylic acid, centrifuged to remove the precipitated protein, and then the intracellular GSH content was measured according to the manufacturer's instructions. The absorbance at 412 nm was measured with a microreader (BIO-RAD Model1680, USA). The GSH level was expressed as the ratio of the mean intensity of the treated group *versus* the mean intensity of the control group.

2.3.5 Malondialdehyde (MDA) measurement. After exposure to the MSNs for 24 h, the cells were scraped off, collected, rinsed with PBS to remove the culture medium, and then resuspended in 0.5% cold Triton X-100. Cell lysates were centrifuged to remove debris, and the supernatants were used for intracellular MDA assays. MDA content was measured with an MDA kit (Jiancheng, Nanjing, China) according to the manufacturer's instructions. The absorbance at 530 was measured with a microreader (BIO-RAD Model1680, USA). The MDA concentration (nmol mg^{-1} protein) in the samples was extrapolated from the standard curve. Results were represented as % change in MDA concentration as compared to the control.

2.3.6 Lactate dehydrogenase (LDH) measurement. LDH leakage is based on the activity measurement of the cytoplasmic enzyme LDH in the extracellular space. At the end of a 24 h exposure to the MSNs, the culture medium was centrifuged and the cell-free supernatant was collected. The activity of LDH in the medium was determined with a commercial LDH kit (Jiancheng, Nanjing, China) according to the manufacturer's protocol. The absorption was measured with a microreader (BIO-RAD Model1680, USA) at 440 nm, and LDH levels in the medium *versus* the cells were quantified and compared to the control.

2.3.7 Statistical analysis. The results are represented as the mean ± standard deviation (SD) (n equals at least 3) and were further analysed by one-way analysis of variance (ANOVA). The comparisons are considered to be significantly different from each other when the p value is smaller than 0.05 and highly significantly different when the p value is smaller than 0.01.

3. Results

3.1 Characterization of MSNs

The surface modified MSNs were prepared by co-condensation of functional trimethoxysilane and tetraethyl orthosilicate, and were characterized with typical techniques. The powder X-ray diffraction (XRD, Fig. S1†) patterns of the MSNs with different surface groups show a typical two-dimensional hexagonal p_6mm mesophase and display the expected features of MCM-41 type mesoporous structure, with the main peaks indexed to the (100) diffraction of a hexagonal structure. Fig. 1 indicates that all the MSNs show highly ordered hexagonally arranged mesopores with one-dimensional channels throughout the particles. A combination of the X-ray patterns and TEM images demonstrates that with the surface

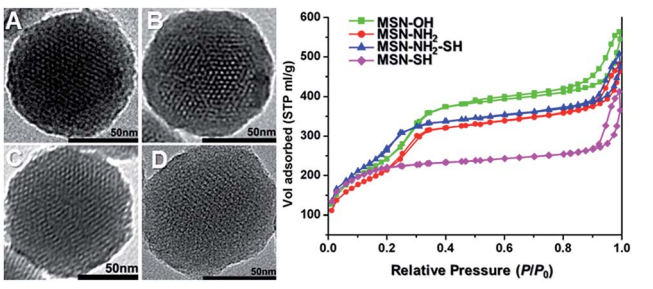

Fig. 1 Transmission electron microscopy (TEM) images (left) of the nanoparticles of MSN–OH (A), MSN–NH_2 (B), MSN–NH_2–SH (C), and MSN–SH (D). BET N_2 adsorption–desorption isotherms (right) of MSN–OH, MSN–NH_2, MSN–NH_2–SH, and MSN–SH at 78 K.

functionalization of the MSNs the mesoporous structure of MCM-41 type silica remains. Generally, the silica nanoparticles tend to aggregate, due to H-bonding interactions between residual silanol groups. This tendency has to be reduced in biological applications, in order to improve cellular uptake, biodistribution, and biocompatibility, *etc.* Though surface modification does not change the mesophase structure of MCM-41, it indeed mediates the surface properties of MCM-41, which was examined with nitrogen adsorption and desorption isotherms at 78 K. The surface properties of the modified MSNs are shown in Fig. 1 and listed in Table 1. Compared with pristine MSN–OH (mean radius: 3.34 nm), thiol-modified MSN–SH has the lowest adsorption capacity and the narrowest channel (mean radius: 2.39 nm). During the fabrication, the functional groups may interact with the micelles upon formation and thus cause a reduction in pore size and shrinkage of the unit cell size. The physicochemical data in Table 1 indicate that the particle size of the modified MSNs is in the range of 200 to 300 nm, and the zeta potential changes dramatically with the groups conjugated on the surface of the MSNs. The zeta potentials are -8.75 ± 3.03, 2.30 ± 0.12, 0.30 ± 0.06 and 3.09 ± 0.25 mV for MSN–OH, MSN–NH_2, MSN–NH_2–SH, and MSN–SH, respectively. When the ligand Tf is conjugated to the MSNs, the value for MSN–Cy–Tf is -6.71 ± 3.03 mV, compared to 35.01 ± 2.12 mV for MSN–Cy.

3.2 BBB permeation potential of the MSNs

The BBB prevents exogenous species from entering the brain from the blood and maintains brain homeostasis.[43] The BBB permeability and brain accumulation of MSN–Cy–Tf and MSN–Cy were examined with *in vivo* fluorescent imaging (Fig. 2) and further confirmed with tissue sectioning (Fig. S2†). *In vivo* fluorescent images were taken at designated time intervals after intravenous tail injection. Surprisingly, the fluorescence of both MSN–Cy–Tf and MSN–Cy was clearly observed in the brains of the treated mice after only 1 min of injection, indicating that both MSN–Cy–Tf and MSN–Cy could enter the brain very quickly (Fig. 2). The accumulation of MSN–Cy in the brain at designated intervals is comparable to that of MSN–Cy–Tf, indicating that the effect of the ligand Tf on the kinetics of the MSNs across the BBB is slight. The concentration of the MSNs gradually decreased several minutes after injection. In addition, the accumulation of the MSNs is also remarkable in the peripheral tissues, such as the kidneys, liver, and spleen. The fluorescence intensity in these tissues implies that the concentration and kinetics of accumulation in the liver, kidneys, and spleen may be higher and faster than that in the brain. Nevertheless, more extensive studies are needed to confirm the permeability and kinetics of the MSNs crossing the BBB and to reveal the mechanism of the MSNs entering the brain.

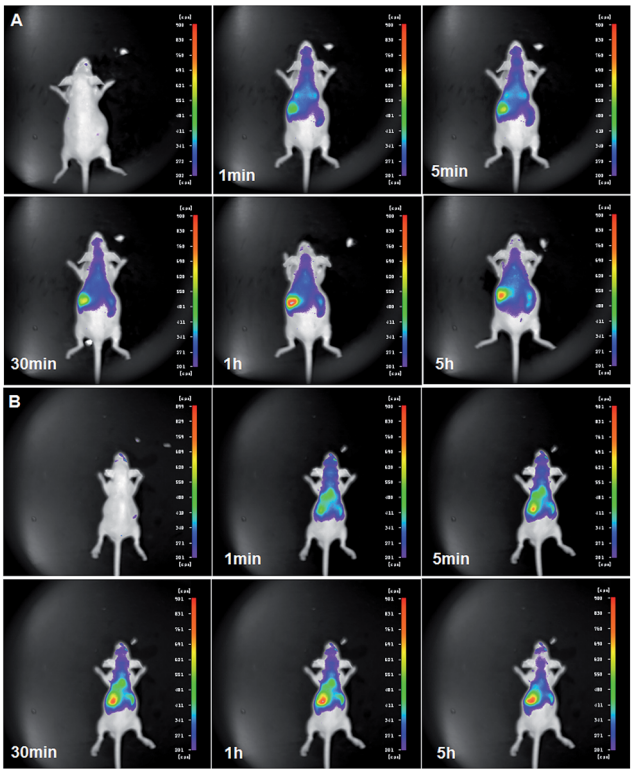

Fig. 2 Distribution of MSNs in nude mice after intravenous tail administration at a dose of 0.1 mL per 10 g (v per body weight). The MSNs were dispersed in 5% glucose to prepare a 1 mg mL^{-1} dose. Images were taken at designated intervals of time after administration. (A) Image of MSN–Cy treated mouse; (B) image of MSN–Cy–Tf treated mouse.

3.3 Histological observation of the hippocampus

In order to further validate the permeability of the MSNs, we selected the hippocampus in the brain as a specific target to observe the effect of the MSN exposure on the neuronal morphological changes by H & E staining. For this purpose, the mice were sacrificed 30 min after injection, taking into account the concentration of the MSNs retained in the brain and the

Table 1 The physicochemical data of functionalized MSNs[a]

MSNs	Radius (nm)	ξ (mV)	Surface area ($m^2\ g^{-1}$)	Pore diameter (nm)
MSN–OH	278.5 ± 8.62	-8.75 ± 3.03	843.17	3.34
MSN–NH_2	266.1 ± 12.0	2.30 ± 0.12	745.31	3.28
MSN–NH_2–SH	271.5 ± 0.42	0.30 ± 0.06	918.31	2.70
MSN–SH	247.4 ± 1.63	3.09 ± 0.25	764.74	2.39

[a] The zeta potential ξ was measured in PBS (0.067 M, pH = 7.4).

time allowed for the interaction between the MSNs and the tissues. Then the brain was excised and subjected to sectioning and staining. Representative images are provided in Fig. 3. In the control group, round and dark stained neurons were arranged approximately layer by layer and packed regularly with the chromatin of the nucleus being stained homogeneously. The neuronal morphological changes in the hippocampus are clear in the MSN–Cy and MSN–Cy–Tf treated groups. The exposure of MSN–Cy and MSN–Cy–Tf evoked a discernible alteration in the hippocampus, which was characterized by neuronal loss and thinning of cell layers, nuclei shrinkage, and disintegration and dark staining of neurons. For the MSN–Cy treated mice, more vacuoles appeared in the hippocampus, compared with that of the MSN–Cy–Tf treated mice. The results of the present study suggest that the MSNs go across the BBB, accumulate in the brain, and damage the neurons of the hippocampus.

3.4 *In vitro* cytotoxicity of various surface modified MSNs

To explore the *in vitro* cytotoxicity of the MSNs, we examined the proliferation of MSN treated PC12 cells, a model for neurobiological studies, with an MTT assay.[44] In brief, PC12 cells were exposed to the modified MSNs at 12.5 μg mL^{-1} to 100 μg mL^{-1} for 24 h. As shown in Fig. 4 the inhibition percentages of MSN–OH, MSN–NH_2 and MSN–NH_2–SH reach a maximum at 50 μg mL^{-1}, while that of MSN–SH reaches a maximum at 100 μg mL^{-1}. The IC_{50} values (50% inhibitory concentration) at 24 h exposure are 5.8, 26.9, 27.1, and 48.7 μg mL^{-1} for MSN–OH, MSN–NH_2, MSN–NH_2–SH, and MSN–SH, respectively, suggesting that the pristine MSN–OH shows the highest cytotoxicity.

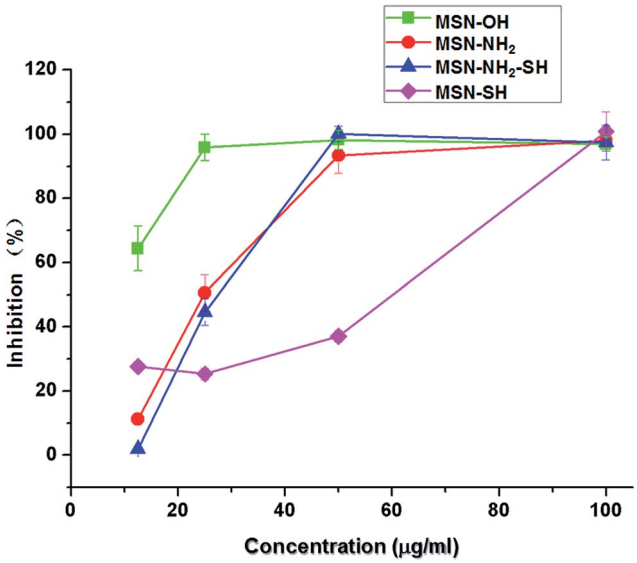

Fig. 4 The concentration dependent cytotoxicity induced by –OH, –NH_2, –NH_2–SH, and –SH modified MSNs. The inhibition rate of various MSNs to PC12 cell was determined with an MTT assay after 24 h exposure. Cells cultured in a medium without MSNs are the control. Data are represented as the mean ± SD ($n = 3$).

3.5 Molecular mechanism of MSNs damaging neurons

To reveal the molecular mechanism of neuronal damage induced by the MSNs, we measured the levels of ROS, GSH, LDH, and MDA in the MSN treated PC12 cells.

3.5.1 ROS elevation of MSN treated PC12 cells. ROS is a collective term for free oxygen radicals, such as superoxide anions, hydroxyl radicals, hydrogen peroxide and ozone. ROS is involved in the pathogenesis of a variety of inflammatory conditions, and an increase of intracellular ROS levels causes damage to the cell structure and eventually results in cell death or apoptosis.[45] The oxidative stress induced by the MSNs on the PC12 cells was assessed by measuring the intracellular ROS level, which was quantified with a DCFH-DA method.[46] The results (Fig. 5) suggest that the ROS elevation induced by the MSNs is surface- and concentration-dependent. MSN–OH and MSN–NH_2 treated cells have the highest ROS levels, which are 2.5-fold higher than that of the control group. However, the ROS levels of the MSN–NH_2–SH and MSN–SH treated cells are equal to that of the control cells. It was also found that, at the IC_{50} concentration, 6 μg mL^{-1} MSN–OH and 27 μg mL^{-1} MSN–NH_2 caused a 2.5-fold increase of intracellular ROS, 27 μg mL^{-1} MSN–NH_2–SH caused a 1.4-fold increase of ROS, and 49 μg mL^{-1} MSN–SH caused only a 1.1-fold increase of ROS. These results imply that the surface effect on the ROS generation is different for the various surface-modified MSNs.

3.5.2 GSH depletion. GSH is a key antioxidant in the body and plays a crucial role in maintaining the homeostasis of

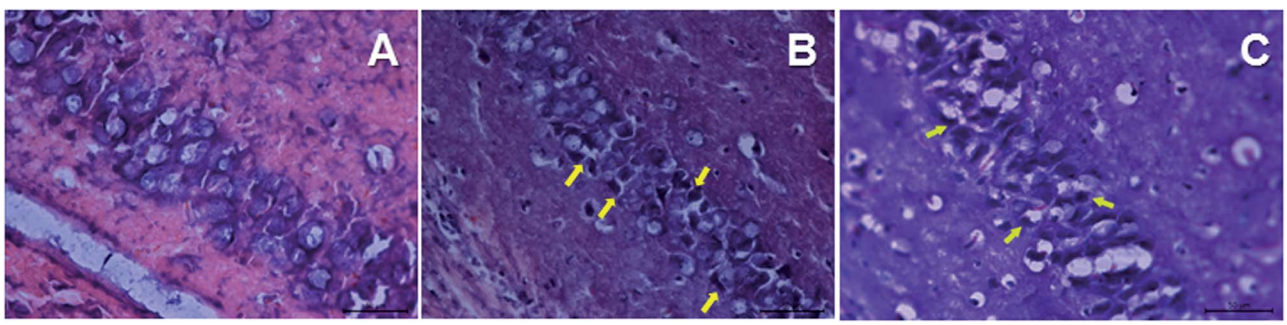

Fig. 3 Neuropathological changes in the hippocampus stained with H & E. (A) Hippocampus of untreated mice (control); (B) hippocampus of MSN–Cy–Tf treated mice; (C) hippocampus of MSN–Cy treated mice. The mice were sacrificed 30 min after injection. The arrows show the dead neuronal cells. The scale bar is 50 μm.

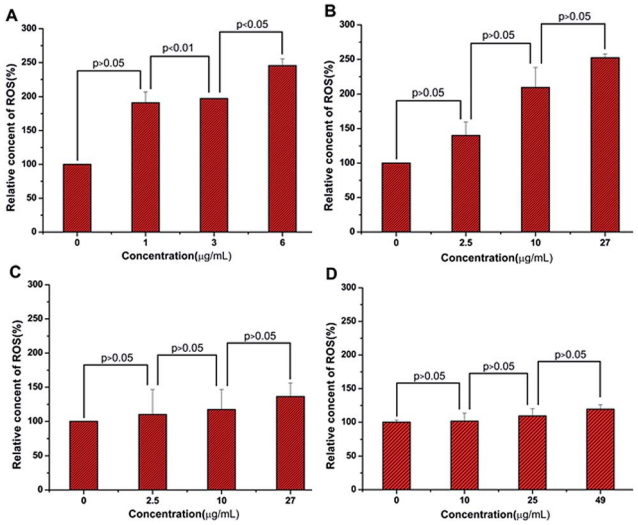

Fig. 5 Effect of the MSNs on ROS elevation. PC12 cells without the MSNs are the control. The PC12 cells were cultured with various concentrations of the MSNs ((A): MSN–OH, (B): MSN–NH_2, (C): MSN–NH_2–SH, and (D): MSN–SH) for 24 h. Intracellular ROS elevation is surface- and concentration-dependent. Data are represented as the mean ± SD ($n = 3$).

cellular oxidation–reduction. Alterations in GSH homeostasis can be considered as an indication of functional damage to the cells, as excessive radicals can give rise to lipid peroxidation and cell membrane damage. As shown in Fig. 6, the effect of the MSNs on intracellular GSH depletion depends on the concentration and surface groups. Relative to the control, 64.6%, 48.0%, 55.9% and 33.2% of intracellular GSH remained for MSN–OH at 6 μg mL^{-1}, MSN–NH_2 at 27 μg mL^{-1}, MSN–NH_2–SH at 27 μg mL^{-1}, and MSN–SH at 49 μg mL^{-1}, respectively.

3.5.3 LDH leakage. LDH is an enzyme widely present in the cytosol that can convert lactate to pyruvate. It will be released into the culture media when the biomembrane integrity is altered or disrupted. The extracellular LDH level depends on the material/chemical toxicity and it is a reflection of the cell membrane integrity. The effects of the surfaces of the MSNs on LDH leakage are shown in Fig. 7. The different surface modified MSNs do not alter the leakage of LDH significantly.

3.5.4 MDA generation. MDA is an end-product of lipid peroxidation and serves as a reliable detection index for lipid peroxidation. The results of the present study (Fig. 8) imply that the MSNs may induce oxidative damage to PC12 cells. All the MSNs show a concentration- and surface-dependent effect on MDA generation. Overall, the generation of MDA for all the MSN treated PC12 cells is 4- to 5-fold higher than that of the control group. For every kind of MSN, the generation of MDA is at the same level in the PC12 cells treated at various concentrations of MSNs, *e.g.* 6 μg mL^{-1} of MSN–OH, 27 μg mL^{-1} of MSN–NH_2, 27 μg mL^{-1} of MSN–NH_2–SH, and 49 μg mL^{-1} of MSN–SH. This indicated that the surface effect is different for the MDA generation.

4. Discussion

Developing CNS drug delivery agents to go across the BBB is a challenging but meaningful task.[47,48] Over the past few years, nanoparticles have shown the potential to overcome the BBB and transport therapeutic agents into the brain *via* intravenous administration and yet the majority of these nanoparticles have been primarily focused toward colloidal carriers, such as liposomes, polymeric nanoparticles, solid

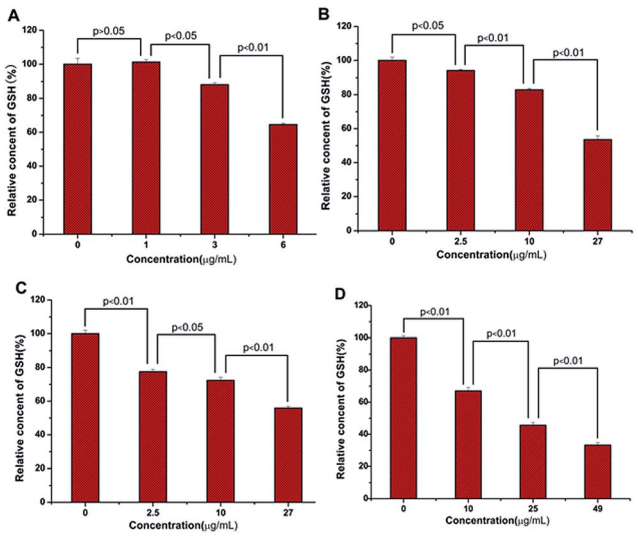

Fig. 6 Effect of the MSNs on GSH reduction. PC12 cells without the MSNs are the control. The PC12 cells were cultured with various concentrations of the MSNs ((A): MSN–OH, (B): MSN–NH_2, (C): MSN–NH_2–SH, and (D): MSN–SH) for 24 h. Intracellular GSH reduction is surface- and concentration-dependent. Data are represented as the mean ± SD ($n = 3$).

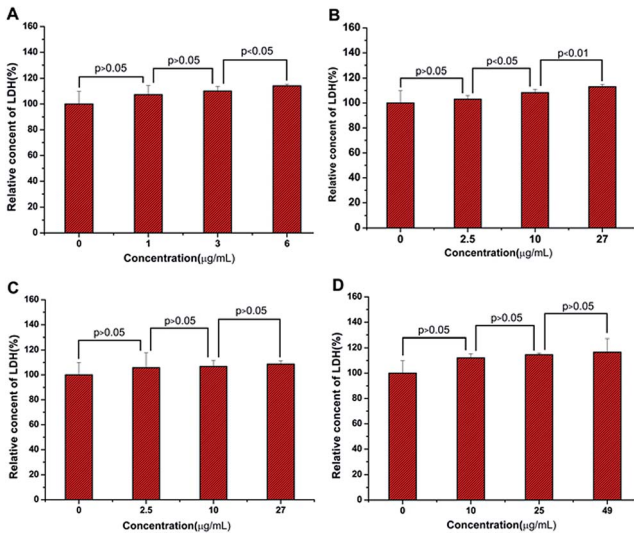

Fig. 7 Effect of the MSNs on LDH leakage. PC12 cells without the MSNs are the control. PC12 cells were cultured with various concentrations of the MSNs ((A): MSN–OH, (B): MSN–NH_2, (C): MSN–NH_2–SH, and (D): MSN–SH) for 24 h. The extracellular LDH content is surface- and concentration-dependent. Data are represented as the mean ± SD ($n = 3$).

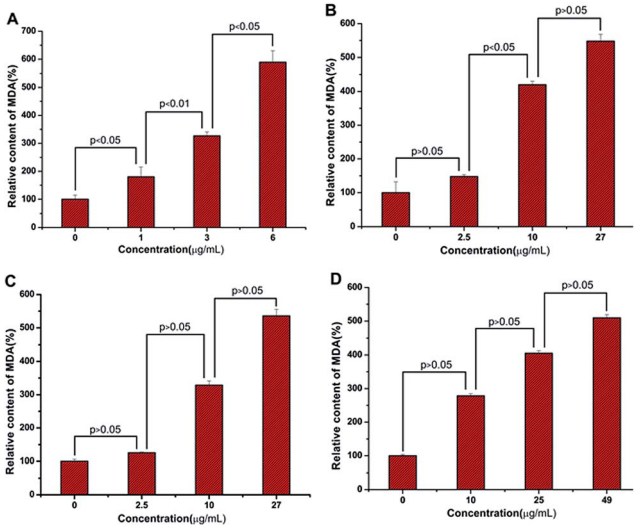

Fig. 8 Effect of the MSNs on MDA production. PC12 cells without the MSNs are the control. PC12 cells were cultured with various concentrations of the MSNs ((A): MSN–OH, (B): MSN–NH_2, (C): MSN–NH_2–SH, and (D): MSN–SH) for 24 h. MDA production is surface- and concentration-dependent. Data are represented as the mean ± SD ($n = 3$).

lipid nanoparticles, polymeric micelles, and dendrimers.[49–52] The most accepted mechanism for the uptake of these nanoparticles into the brain appears to be transcytosis mediated by specific receptors expressed at the BBB, such as lipoproteins, transferrin receptors and insulin receptors.[51,53] In our present work, *in vivo* imaging indicates that even the MSNs without Tf modification may go across the BBB and enter the brain.

The mechanism by which nanoparticles cross the BBB depends on the materials' structural and physicochemical properties, such as the particle size, charge/surface potential, H-bonding potential, and lipophilicity, *etc.*[54] Most of the successful exemplary nanoparticles used to deliver various drugs into the brain range in size from 150 to 300 nm, which may affect the endocytic uptake mechanism.[55] The surface charge and hydrophobicity also influence the uptake. Generally, non-ionic and hydrophobic surfaces are rapidly opsonized followed by recognition by the reticular endothelial system, and higher internalization rates are usually associated with positively charged particles because of the negatively charged components of the cell membranes.[56,57] However, negatively charged nanoparticles can also yield efficient uptake, especially after adsorption or covalent coupling of targeting ligands.[58] MSN–Cy–Tf (253.6 ± 7.50 nm) and MSN–Cy (257.1 ± 2.97 nm), used in this study, have zeta potentials of −6.71 ± 3.03 mV and 35.01 ± 2.12 mV, respectively. It seems that both the zeta potential and particle size influence the uptake of the nanoparticles.[59–61] Further study is needed to elucidate the mechanism of the nanoparticles entering the brain.

Risks are associated with the MSNs entering in the brain. Therefore, it is meaningful to demonstrate the possibility of the accumulation of the MSNs in the brain. Herein we performed a histopathological observation of the hippocampus, a typical tissue of the brain and a critical integration centre for cognitive functions such as learning and memory. ROS can trigger deleterious effects in the brain[62,63] because excessive ROS could result in lipid peroxidation in the hippocampus, striatum, and frontal cortex, *etc.*[64,65] The hippocampus is particularly sensitive to lipid peroxidation due to its high levels of polyunsaturated fatty acids and iron,[63] both of which are a target of free radicals. In addition, the hippocampus possesses low levels of antioxidants.[66] As the cells at the portal-of-entry sites in the brain, the neuronal response to the MSN exposure was morphologically examined. The morphological changes, such as neuronal nuclear shrinkage, vacuole appearance and necrotic neurons in the hippocampus indicate risks of neuronal damage and neurotoxicity from MSN–Cy and MSN–Cy–Tf treatment. With respect to neuronal damage, the damage by MSN–Cy is more severe than that by MSN–Cy–Tf, possibly due to the more positive surface charge and therefore stronger interaction of MSN–Cy with the negatively charged cell membrane.[56,57,67]

The most discussed example for the toxicity of nanomaterials is oxidative stress,[68–73] attributed to ROS elevation. Some *in vivo* studies have demonstrated that nanomaterials can cross the BBB and accumulate in the brain causing CNS damage, of which oxidative stress is vital and important.[74,75] It has been well-established that ROS production and oxidative stress play a crucial role in the important mechanisms involved in the effects of both micro- and nano-sized crystalline or amorphous silicon and silica materials.[26,76–81] Generally, the prime toxicity of silica materials is attributed to surface radicals ($SiO^{\bullet}$, $SiO_2^{\bullet}$, $SiO_3^{\bullet}$ and $Si + O_2^{\bullet-}$), which can react with water to yield ROS, and thus result in oxidative stress to damage DNA and proteins[8,34,82,83] and then affect cell cycle progression *via* initiating apoptosis. In addition, through H-bonding and electrostatic interactions with the biomembrane components the MSNs can cause toxic reactions.[84] In this study, we used PC12 cells to investigate the potential neurotoxicity of the MSNs and to explain the mechanisms of neurotoxicity by correlating the surface modification with oxidative stress indicated by the levels of ROS, GSH, LDH, and MDA.

The MTT assay of PC12 cells exposed to MSN–OH, MSN–NH_2, MSN–NH_2–SH, and MSN–SH for 24 h showed a concentration-dependent toxicity. MSN–OH, MSN–NH_2, and MSN–NH_2–SH show severe cytotoxicity at 50 μg mL^{-1}, with the inhibition higher than 90%. Though MSN–SH at 12.5 μg mL^{-1} shows high inhibition, it shows the lowest inhibition among the test MSNs at 25 to ~50 μg mL^{-1}. Of the four kinds of MSNs, MSN–OH shows the severest cytotoxicity whereas MSN–SH shows the lowest cytotoxicity, as indicated by the IC_{50} values, of which that of MSN–OH is 7-fold lower than that of MSN–SH. Since the sizes and shapes of the MSNs used in this work are identical, the effect of the size and shape on the cytotoxicity is disregarded. With respect to the surface charge and hydroxyl coverage, MSN–OH has the most profound negative potential and the largest hydroxyl coverage. In addition to the intrinsic presence of surface

radicals and ROS generation, the H-bonding and electrostatic interactions of the MSNs with the biomembrane should also contribute to the cytotoxicity. In contrast, MSN–SH could provide a reductive thiol to alleviate the oxidative stress and damage, giving rise to the low cytotoxicity.

It is known that many intracellular redox processes are driven by the redox properties of thiol groups, and intracellular protection against oxidation can be mediated by thiol–disulfide exchange between inflow thiol and oxidized glutathione.[85,86] After MSN–SH is internalized by PC12 cells, the radicals $SiO^{\bullet}$, $SiO_2^{\bullet}$, $SiO_3^{\bullet}$ and $Si + O_2^{\bullet-}$ from the silica surface could generate reactive $HO^{\bullet}$ radicals and induce oxidative stress. When the GSSG (glutathione disulfide)/GSH ratio rises, the depletion of GSH could be prevented by the thiol group of MSN–SH, giving rise to the regeneration of GSH through exchange of the thiol of MSN–SH with GSSG. The highest IC_{50} and the lowest oxidative stress of MSN–SH on the treated PC12 cells suggest that MSN–SH is able to reduce GSSG to GSH through a nonenzymatic thiol–disulfide exchange and protect the cells from the oxidative stress, thereby alleviating the neurotoxicity.

To correlate the cytotoxicity with oxidative stress, we examined the oxidative stress biomarkers, LDH, ROS, MDA, and GSH. The LDH level in the media can be an indicator of cytotoxicity, because damage to the biomembranes can trigger the release of intracellular LDH, which induces a chain reaction of further cell death.[87] It was found that the cytotoxicity indicated by the LDH level and the oxidative stress indexed by ROS, MDA, and GSH are linearly correlated to each other (Fig. S3†). In most cases the correlation coefficient R^2 is larger than 0.95 (Table 2), suggesting that the cytotoxicity appears to be strongly relevant to the oxidative stress manifested by elevated ROS, depleted GSH, and increased MDA. The elevation of ROS seems to deplete cellular GSH significantly, induce lipid peroxidation, produce MDA, alter the biomembrane integrity, result in LDH leakage, and eventually lead to cell death. Excessive ROS in PC12 cells directly oxidizes DNA, proteins, and lipids, thereby damaging the biomembranes and its functions, consequently being associated with the activation of apoptosis.[8,63] It is known that apoptosis can be triggered at the mitochondria, cell membrane receptors and chromosomal DNA.[88] MTT and LDH measurements in this work suggest mitochondrial injury, which may be produced by oxidative stress. In response to these death stimuli, the mitochondria may initiate programmed cell death and apoptosis.[89,90]

Table 2 R^2 of the correlation between LDH levels and ROS, GSH, and MDA levels, respectively

Samples	ROS *versus* LDH	GSH *versus* LDH	MDA *versus* LDH
MSN–OH	0.9078	0.9973	0.9973
MSN–NH_2	0.9883	0.9252	0.9676
MSN–NH_2–SH	0.9946	0.9855	0.9719
MSN–SH	0.9803	0.9922	0.9999

5. Conclusions

In summary, we performed an *in vivo* imaging experiment to examine the potential of MSNs to cross the BBB with or without the ligand Tf and the direct biological effects of the MSNs on PC12 cells, and the neurotoxicity of the MSNs was also explored. The *in vivo* results suggest that the MSNs may go across the BBB, accumulate in the brain, and induce hippocampal neuronal damage. The *in vitro* exposure of the MSNs resulted in morphological cellular changes and oxidative stress, as indicated by the elevation of intracellular ROS which triggered cell death in a concentration-dependent manner, as well as GSH depletion, MDA generation, and LDH leakage. The association of oxidative stress with the cytotoxicity caused by the various MSNs correlates the surface chemistry with the oxidative stress and thus the neurotoxicity. Further studies are needed to address the mechanism of the internalization and oxidative stress to reveal the basis of the neurotoxicity induced by the MSNs. The present study sheds light on the possibility of mediating the neurotoxicity *via* the surface modification of the MSNs in biomedical applications.

Acknowledgements

The authors thank the NSFC (21171120, 21571133), Natural Science Foundation of Beijing Municipality (7132020), Beijing Municipal Science & Technology Commission (Z141100002114049), and TJSHG (201310025008) for financial support.

Notes and references

1 P. Blasi, S. Giovagnoli, A. Schoubben, M. Ricci and C. Rossi, *Adv. Drug Delivery Rev.*, 2007, **38**, 454–477.
2 W. M. Pardridge, *Curr. Opin. Pharmacol.*, 2006, **6**, 494–500.
3 W. G. Kreyling, M. Semmler-Behnke, S. Takenaka and W. Möller, *Acc. Chem. Res.*, 2013, **43, 714-722**.
4 T. R. Pisanic, *Biomaterials*, 2007, **28**, 2572–2581.
5 S. M. Hussain, A. K. Javorina, A. M. Schrand, H. M. Duhart, S. F. Ali and J. J. Schlager, *Toxicol. Sci.*, 2006, **92**, 456–463.
6 E. Gitto, R. J. Reiter, M. Karbownik, D. Tan, P. Gitto, S. Barberi and I. Barberi, *Biol. Neonate*, 2002, **81**, 146–157.
7 R. Piga, Y. Saito, Y. Yoshida and E. Niki, *Neurotoxicology*, 2007, **28**, 67–75.
8 J. F. Turrens, *J. Physiol.*, 2003, **552**, 335–344.
9 K. J. Barnham, C. L. Masters and A. I. Bush, *Nat. Rev. Drug Discovery*, 2004, **3**, 205–214.
10 A. A. C. Suzy and C. E. Serpil, *Am. J. Physiol.: Lung Cell. Mol. Physiol.*, 2002, **283**, 246–255.
11 D. Trachootham, J. Alexandre and P. Huang, *Nat. Rev. Drug Discovery*, 2009, **8**, 579–591.
12 J. S. Beck, J. C. Vartuli, W. J. Roth, M. E. Leonowicz, C. T. Kresge, K. D. Schmitt, C. T. W. Chu, D. H. Olson and E. W. Sheppard, *J. Am. Chem. Soc.*, 1992, **114**, 10834–10843.
13 B. G. Trewyn, I. I. Slowing, S. Giri, H. T. Chen and V. S. Y. Lin, *Acc. Chem. Res.*, 2007, **40**, 846–853.
14 Z. Tao, *RSC Adv.*, 2014, **4**, 18961.

15 M. Vallet-Regi, F. Balas and D. Arcos, *Angew. Chem., Int. Ed.*, 2007, **46**, 7548–7558.
16 J. E. Lee, N. Lee, T. Kim, J. Kim and T. Hyeon, *Acc. Chem. Res.*, 2011, **44**, 893–902.
17 M. W. Ambrogio, C. R. Thomas, Y.-L. Zhao, J. I. Zink and J. F. Stoddart, *Acc. Chem. Res.*, 2011, **44**, 903–913.
18 I. I. Slowing, J. L. Vivero-Escoto, C.-W. Wu and V. S.-Y. Lin, *Adv. Drug Delivery Rev.*, 2008, **60**, 1278–1288.
19 Q. He and J. Shi, *Adv. Mater.*, 2014, **26**, 391–411.
20 D. Tarn, C. E. Ashley, M. Xue, E. C. Carnes, J. I. Zink and C. J. Brinker, *Acc. Chem. Res.*, 2013, **46**, 792–801.
21 A. Popat, S. B. Hartono, F. Stahr, J. Liu, S. Z. Qiao and G. Q. Lu, *Nanoscale*, 2011, **3**, 2801.
22 J. M. Rosenholm, C. Sahlgren and M. Lindén, *Nanoscale*, 2010, **2**, 1870–1883.
23 V. Castranova and V. Vallyathan, *Environ. Health Perspect.*, 2000, **108**(suppl. 4), 3–14.
24 K. Donaldson and P. J. A. Borm, *Ann. Occup. Hyg.*, 1998, **42**, 287–294.
25 B. Rimal, A. K. Greenberg and W. N. Rom, *Curr. Opin. Pulm. Med.*, 2005, **11**, 169–173.
26 D. Napierska, L. C. J. Thomassen, D. Lison, J. A. Martens and P. H. Hoet, *Part. Fibre Toxicol.*, 2010, **7**, 39.
27 V. Castranova, V. Vallyathan and W. E. Wallace, *Silica and silica-induced lung diseases*, CRC Press, 1996.
28 G. M. Calvert, F. L. Rice, J. M. Boiano, J. W. Sheehy and W. T. Sanderson, *Occup. Environ. Med.*, 2003, **60**, 122–129.
29 D. D. Dunnom, *Health effects of syntheticsilica particulates : a symposium*, American Society for Testing and Materials, 1981.
30 J. K. Mclaughlin, W. H. Chow and L. S. Levy, *J. Toxicol. Environ. Health*, 1997, **50**, 553–566.
31 I. Roy, T. Y. Ohulchanskyy, D. J. Bharali, H. E. Pudavar, R. A. Mistretta, N. Kaur and P. N. Prasad, *Proc. Natl. Acad. Sci. U. S. A.*, 2005, **102**, 279–284.
32 D. J. Bharali, I. Klejbor, E. K. Stachowiak, P. Dutta, I. Roy, N. Kaur, E. J. Bergey, P. N. Prasad and M. K. Stachowiak, *Proc. Natl. Acad. Sci. U. S. A.*, 2005, **102**, 11539–11544.
33 J. Choi, Q. Zheng, H. E. Katz and T. R. Guilarte, *Environ. Health Perspect.*, 2010, **118**, 589–595.
34 J. Wu, C. Wang, J. Sun and Y. Xue, *ACS Nano*, 2011, **5**, 4476–4489.
35 M. Huan, X. Min, T. Xia, Z. Ji, D. Y. Tarn, J. I. Zink and A. E. Nel, *ACS Nano*, 2011, 4131–4144.
36 G. Oberdörster, E. Oberdörster and J. Oberdörster, *Environ. Health Perspect.*, 2005, **113**, 823–839.
37 S. K. Natarajan and S. Selvaraj, *RSC Adv.*, 2014, **4**, 14328.
38 I. Fenoglio, G. Martra, S. Coluccia and B. Fubini, *Chem. Res. Toxicol.*, 2000, **13**, 971–975.
39 K. M. Waters, L. M. Masiello, R. C. Zangar, B. J. Tarasevich, N. J. Karin, R. D. Quesenberry, S. Bandyopadhyay, J. G. Teeguarden, J. G. Pounds and B. D. Thrall, *Toxicol. Sci.*, 2009, **107**, 553–569.
40 M. Cho, W.-S. Cho, S. J. Kim, B. S. Han, S. H. Kim, Y. Y. Sheen and J. Jeong, *Toxicol. Lett.*, 2009, **189**, 177–183.
41 R. Guo, L. L. Li, W. H. Zhao, Y. X. Chen, X. Z. Wang, C. J. Fang, W. Feng, T. L. Zhang, X. Ma, M. Lu, S. Q. Peng and C. H. Yan, *Nanoscale*, 2012, **4**, 3577–3583.
42 W. Wang, C. Fang, X. Wang, Y. Chen, Y. Wang, W. Feng, C. Yan, M. Zhao and S. Peng, *Nanoscale*, 2013, **5**, 6249–6253.
43 N. J. Abbott, A. A. Patabendige, D. E. Dolman, S. R. Yusof and D. J. Begley, *Neurobiol. Dis.*, 2010, **37**, 13–25.
44 T. Ishima, T. Nishimura, M. Iyo and K. Hashimoto, *Prog. Neuro-Psychopharmacol. Biol. Psychiatry*, 2008, **32**, 1656–1659.
45 M. Ott, V. Gogvadze, S. Orrenius and B. Zhivotovsky, *Apoptosis*, 2007, **12**, 913–922.
46 *Identification of ROS Using Oxidized DCFDA and Flow-Cytometry*, ed. E. Eruslanov and S. Kusmartsev, Humana Press, London, 2010.
47 H. B. Newton, *Expert Rev. Neurother.*, 2006, **6**, 1495–1509.
48 J. F. Deeken, *Clin. Cancer Res.*, 2007, 1663–1674.
49 S. B. Tiwari and M. M. Amiji, *Curr. Drug Delivery*, 2006, **3**, 219–232.
50 R. Alyautdin, I. Khalin, M. I. Nafeeza, M. H. Haron and D. Kuznetsov, *Int. J. Nanomed.*, 2014, **9**, 795–811.
51 S. R. Hwang and K. Kim, *Arch. Pharmacal Res.*, 2014, **37**, 24–30.
52 P. Blasi, S. Giovagnoli, A. Schoubben, M. Ricci and C. Rossi, *Adv. Drug Delivery Rev.*, 2007, **59**, 454–477.
53 G. Reinhard, *Neurobiol. Dis.*, 2009, **37**, 48–57.
54 M. P. Giovanne, *Pharm. Res.*, 1997, **14**, 164–168.
55 S. Wohlfart, S. Gelperina and J. Kreuter, *J. Controlled Release*, 2012, **161**, 264–273.
56 Y. Oh and J. Swanson, *J. Cell Biol.*, 1996, **132**, 132–585.
57 C. Foged, B. Brodin, S. Frokjaer and A. Sundblad, *Int. J. Pharm.*, 2005, **298**, 315–322.
58 H. Hillaireau and P. Couvreur, *CMLS, Cell. Mol. Life Sci.*, 2009, **66**, 2873–2896.
59 P. R. Lockman, *Drug Dev. Ind. Pharm.*, 2002, **28**, 1–13.
60 M. Malakoutikhah, M. Teixidó and E. Giralt, *Angew. Chem., Int. Ed. Engl.*, 2011, **50**, 7998–8014.
61 I. van Rooy, E. Mastrobattista, G. Storm, W. E. Hennink and R. M. Schiffelers, *J. Controlled Release*, 2011, **150**, 30–36.
62 C. M. Bergamini, S. Gambetti, A. Dondi and C. Cervellati, *Curr. Pharm. Des.*, 2004, **10**, 1611–1626.
63 B. Halliwell and J. M. C. Gutteridge, *Free Radicals in Biology and Medicine*, Oxford University Press, 2007.
64 M. F. Rivelilson, M. M. V. Silvânia, C. F. S. Francisca, S. B. V. Glauce and M. F. F. Marta, *FEBS J.*, 2005, **272**, 1307–1312.
65 H. Daniel and W. G. M. B. Hendrikus, *Trends Pharmacol. Sci.*, 1993, **14**, 270–275.
66 T. Kishido, K. Unno, H. Yoshida, D. Choba, R. Fukutomi, S. Asahina, K. Iguchi, N. Oku and M. Hoshino, *Biogerontology*, 2007, **8**, 423–430.
67 D. Drescher, G. Orts-Gil, G. Laube, K. Natte, R. W. Veh, W. Österle and J. Kneipp, *Anal. Bioanal. Chem.*, 2011, **400**, 1367–1373.
68 T. Xia, M. Kovochich, J. Brant, M. Hotze, J. Sempf, T. Oberley, C. Sioutas, J. I. Yeh, M. R. Wiesner and A. E. Nel, *Nano Lett.*, 2006, **6**, 1794–1807.
69 H. Meng, T. Xia, S. George and A. E. Nel, *ACS Nano*, 2009, **3**, 1620–1627.

70 J. Shi, H. L. Karlsson, K. Johansson, V. Gogvadze, L. Xiao, J. Li, T. Burks, A. Garcia-Bennett, A. Uheida, M. Muhammed, S. Mathur, R. Morgenstern, V. E. Kagan and B. Fadeel, *ACS Nano*, 2012, **6**, 1925–1938.
71 S. J. Soenen, W. J. Parak, J. Rejman and B. Manshian, *Chem. Rev.*, 2015, **115**, 2109–2135.
72 V. Stone, H. Johnston and M. J. Clift, *IEEE Transactions on NanoBioscience*, 2007, **6**, 331–340.
73 A. A. Shvedova, E. Kisin, A. R. Murray, V. J. Johnson, O. Gorelik, S. Arepalli, A. F. Hubbs, R. R. Mercer, P. Keohavong and N. Sussman, *Am. J. Physiol.: Lung Cell. Mol. Physiol.*, 2008, **295**, L552–L565.
74 G. Oberdörster, Z. Sharp, V. Atudorei, A. Elder, R. Gelein, W. Kreyling and C. Cox, *Inhalation Toxicol.*, 2004, **16**, 437–445.
75 L. An, S. Liu, Z. Yang and T. Zhang, *Toxicol. Lett.*, 2012, **213**, 220–227.
76 P. Eun-Jung and P. Kwangsik, *Toxicol. Lett.*, 2009, **184**, 18–25.
77 R. Kumar, I. Roy, T. Y. Ohulchanskky, L. A. Vathy, E. J. Bergy, M. Sajjad and P. N. Prasad, *ACS Nano*, 2010, **4**, 699–708.
78 S. J. So, I. S. Jang and C. S. Han, *J. Nanosci. Nanotechnol.*, 2008, **8**, 5367–5371.
79 J. Jiang, K. Huo, S. Chen, Y. Xin, Y. Xu, Z. Wu, Z. Yu and P. Chu, *Biomaterials*, 2009, **30**, 2661–2665.
80 H. A. Santos, J. Riikonen, J. Salonen, E. Makila, T. Heikkila, T. Laaksonen, L. Peltonen, V. P. Lehto and J. Hirvonen, *Acta Biomater.*, 2010, **6**, 2721–2731.
81 B. Fubini and A. Hubbard, *Free Radical Biol. Med.*, 2003, **34**, 1507–1516.
82 J. A. Imlay and S. Linn, *Science*, 1988, **240**, 1302–1309.
83 B. Halliwell, *Am. J. Med.*, 1991, **91**, 14–22.
84 I. Slowing, C. W. Wu, J. L. Vivero-Escoto and V. S. Lin, *Small*, 2009, **5**, 57–62.
85 A. Holmgren, C. Johansson, C. Berndt, M. E. Lönn, C. Hudemann and C. H. Lillig, *Biochem. Soc. Trans.*, 2005, **33**, 13963–13966.
86 M. B. Toledano, C. Kumar, N. L. Moan, D. Spector and F. Tacnet, *FEBS Lett.*, 2007, **581**, 3598–3607.
87 C. M. Sayes, A. M. Gobin, K. D. Ausman, J. Mendez, J. L. West and V. L. Colvin, *Biomaterials*, 2005, **26**, 7587–7595.
88 S. H. Graham and J. Chen, *J. Cereb. Blood Flow Metab.*, 2001, **21**, 99–109.
89 J. C. Reed, *J. Cell Biol.*, 1994, **124**, 1–6.
90 J. C. Reed, J. M. Jurgensmeier and S. Matsuyama, *Biochim. Biophys. Acta*, 1998, **1366**, 127–137.